Heteroepitaxial Hexagonal (00.1) $CuFeO_2$ Thin Film Grown on Cubic (001) $SrTiO_3$ Substrate through Translational and Rotational Domain Matching

Sijun Luo, George F. Harrington*, Kuan-Ting Wu, Daniele Pergolesi, and Thomas Lippert**

Dr. S. Luo, Dr. G. F. Harrington, Dr. K.-T. Wu, Prof. T. Lippert
International Institute for Carbon-Neutral Energy Research (WPI-I^2CNER),
Kyushu University, 744 Motooka, Fukuoka 819-0395, Japan
E-mail: joeney.rowe@yahoo.com; harrington.frederick.george.302@m.kyushu-u.ac.jp; thomas.lippert@psi.ch

Dr. S. Luo, Dr. D. Pergolesi, Prof. T. Lippert
Laboratory for Multiscale Materials Experiments,
Paul Scherrer Institute, 5232 Villigen PSI, Switzerland

Dr. G. F. Harrington
Center of Coevolutionary Research for Sustainable Communities (C2RSC),
Kyushu University, 744 Motooka, Fukuoka 819-0395, Japan

Dr. G. F. Harrington
Department of Materials Science and Engineering,
Massachusetts Institute of Technology, Massachusetts 02139, United States

Prof. T. Lippert
Laboratory of Inorganic Chemistry, Department of Chemistry and Applied Biosciences,
ETH Zurich, 8093 Zurich, Switzerland

Keywords: heteroepitaxial thin films, rotational domain matching, $CuFeO_2$, $SrTiO_3$

Heteroepitaxy of complex oxide thin films is a significant challenge when a large mismatch in the lattice parameters (> 8 %) and difference in the crystallographic symmetry coexist between the film and substrate. This work reports the heteroepitaxial growth of a hexagonal delafossite $CuFeO_2$ thin film with (00.1) orientation on a cubic perovskite (001) SrTiO3 substrate through translational and rotational domain matching epitaxy. The rotational in-plane domain orientation relationships are $CuFeO_2$ [11.0] // $SrTiO_3$ [110] and $CuFeO_2$ [2-1.0] // $SrTiO_3$ [110] with about 10 % in-plane lattice mismatch. The 14.8 nm thick (00.1) $CuFeO_2$ thin film shows high crystalline quality with a full width at half maximum of rocking curve of about 0.24 degrees and exhibits a possible indirect optical bandgap of 1.43 eV or direct optical bandgap of 1.94 eV. This study not only reports a model system demonstrating translational and rotational domain matching heteroepitaxy of complex oxides, but

also opens a way to thin film heterostructures integrating hexagonal delafossite with cubic perovskite materials for functional oxide devices.

Hexagonal $CuFeO_2$ with the delafossite structure, well-known for its antiferromagnetic and multiferroic properties at low temperature, has garnered attention in studies of p-type oxide semiconductor for potential opto-electronic applications in photoelectrochemistry since 1987,[1] and recently in photodiode devices.[2-4] $CuFeO_2$ has recently attracted extensive interest as a promising narrow-band-gap semiconductor photocathode material for solar fuel conversion,[5-14] due to the tunable and relative small optical bandgap (Eg ~ 1.5 eV) with the position of the conduction/valence bands in a useful range. In addition, $CuFeO_2$ consists of earth-abundant Cu and Fe elements, which is important for applications. Conventional photoanodes typically consist of powders of the photo-active material deposited by electrophoretic deposition on a conductive substrate, which is needed as the current collector for the standard photoelectrochemical (PEC) test. However, the development of performing photoelectrodes for visible light-driven water splitting and CO_2 reduction has enormous advantages by the use of thin films deposition technology.[15,16] Thin films can indeed be used as ideal model systems, with well-defined crystalline, crystallographic, and morphological properties, to access subtle materials' properties whose characterization would be precluded with conventional samples. Particularly important is for example the role of the crystallographic surface and bulk orientation which can affect the charge transfer at the solid/liquid interface and the external quantum efficiency.[17-19] Crystalline, epitaxial thin films, of $CuFeO_2$ grown on conducting substrates, is an alternative device design that would allow us to gain complementary insights into the PEC properties of this promising material.

It is beneficial to study the fundamental physics and chemistry of thin film $CuFeO_2$ for possible technological applications. It is, therefore, desirable to deposit high-quality thin films with specific crystallographic orientation on commercial conductive single crystal substrates or conductive epitaxial layer-buffered single crystal substrates. The cubic perovskite $SrTiO_3$

doped with Nb is the only commercially available conductive single crystal metal oxide substrate widely used for growing epitaxial oxide thin films. Alternatively, epitaxial layers of cubic perovskite oxides, such as $SrRuO_3$,[20-22] $La_xSr_{1-x}MnO_3$,[23,24] $LaNiO_3$,[25-27] and $SrMoO_3$,[27-30] are commonly used as conductive buffer layers. The epitaxial growth of $CuFeO_2$ thin film has been only demonstrated with a (00.1) out-of-plane crystallographic orientation on insulating hexagonal (00.1) sapphire substrates using pulsed laser deposition.[31,32] There is no report on heteroepitaxy formed between the crystal planes of hexagonal delafossite and cubic perovskite materials. The heteroepitaxial growth of $CuFeO_2$ thin films on cubic perovskite $SrTiO_3$ substrates would not only create a platform to study the fundamental photoelectrochemical properties of $CuFeO_2$, but also provide a model system to demonstrate the feasibility of oxide heterostructures consisting of the two functional complex oxide families for developing oxide-based devices with novel functionalities.

Owing to the similar crystal symmetry, a heteroepitaxial interface between cubic (111) crystal plane and hexagonal (00.1) crystal plane can be obtained, and several examples are reported in leterature.[33-38] The few examples of heteroepitaxy between cubic (001) and hexagonal (00.1) planes of metal oxides are La(Sr)MnO_3 (001) [110] // ZnO (00.1) [10.0],[36] and $BaTiO_3$ (001) [110] // ZnO (00.1) [10.0],[39-41] in which the occurrence of domain rotations is the consequence of mismatch of the rotational symmetries of the cubic (100) and hexagonal (00.1) crystal planes.[41] And both cases are characterized by a relatively small in-plane lattice mismatch along the [110] // [10.0] directions of about 2 % and 0.5 %, respectively. However, in the case of interest for the present study, the lattice mismatch between hexagonal (00.1) $CuFeO_2$ (a=3.033 Å, both Fe-Fe and O-O distances are 3.033 Å) and cubic (001) $SrTiO_3$ (a=3.905 Å, O-O minimum distance is 2.761 Å) is about 10 %,[42,43] which is far too large to allow heteroepitaxial growth with a coherent interface.

In systems with a large lattice misfit of above 8 %, the film and substrate with similar crystal symmetry may form a heteroepitaxial interface through domain matching epitaxy, where

a periodic array of dislocations forms along the interface to accommodate the lattice mismatch.[44] In some cases, a structurally-modified transition layer has been reported to be formed at the interface to facilitate the heteroepitaxial growth.[45,46] Recently, domain matching epitaxy was observed for orthorhombic (111) $Hf_{0.5}Zr_{0.5}O_2$ (HZO) thin films grown on cubic (001) $La_{2/3}Sr_{1/3}MnO_3$ (LSMO) epitaxial layer through the introduction of arrays of interface dislocations with short periodic spacing.[47] In this unique case, the crystal planes of the film and substrate show an apparent symmetry dissimilarity, while the lattice mismatches along two in-plane matching orientations of HZO [-211] // LSMO [1-10] and HZO [0-22] // LSMO [1-10] are calculated to be about 10 % and 58 %, respectively. Although the domain rotational heteroepitaxy could form between the two crystal planes without symmetry similarity, typical examples are normally observed only for systems with small lattice mismatch.[41] The complex chemical interface composition and chemical interactions, together with large lattice mismatches and dissimilar crystal symmetries, makes heteroepitaxy of complex oxides systems very challenging. To date, the examples of heteroepitaxial growth of complex oxides thin films with symmetry dissimilarity and large lattice mismatch (above 8 %) are limited.

Understanding the interfacial structures in complex oxide heterostructure systems with symmetry dissimilarity and large lattice mismatch is crucial for studying complex oxide heterostructures and developing oxide thin film devices. The $CuFeO_2/SrTiO_3$ heterostructure can indeed be considered as a proto-typical example of this kind of oxide heterostructures. This work demonstrates the heteroepitaxy of a hexagonal (00.1) $CuFeO_2$ thin film grown on a cubic (001) $SrTiO_3$ substrate through translational and rotational domain matching epitaxy.

The $CuFeO_2$ thin films were grown on single crystal (001) $SrTiO_3$ substrates using pulsed laser deposition (PLD). The preparation of the $CuFeO_2$ bulk target for PLD and the effects of deposition parameter on the growth of $CuFeO_2$ thin films are reported in our previous work on heteroepitaxial (00.1) $CuFeO_2$ films grown on sapphire substrates.[32] We have selected the film thickness of 14.8 nm because we could show in our previous work,[32] that pure phase (00.1)

$CuFeO_2$ epitaxial films grown on (00.1) sapphire substrates could only be obtained with a maximum film thickness of about 16 nm, above which a second phase of Fe_2O_3 nanograins is formed. As we used the same PLD conditions in the present study, to grow the epitaxial (00.1) $CuFeO_2$ thin films on (001) $SrTiO_3$ substrates, we limited the film thickness to less than 16 nm, to achieve the heteroepitaxy between hexagonal (00.1) delafossite and cubic (001) perovskite crystal planes through translational and rotational domain matching. In this work, the thin film deposition was performed using a laser fluence of 3.5 J cm^{-2} with a 3 Hz repetition rate for a deposition time of 40 minutes. The oxygen partial pressure was kept at 0.07 Pa and the substrate was held at a set temperature of 900 ℃.

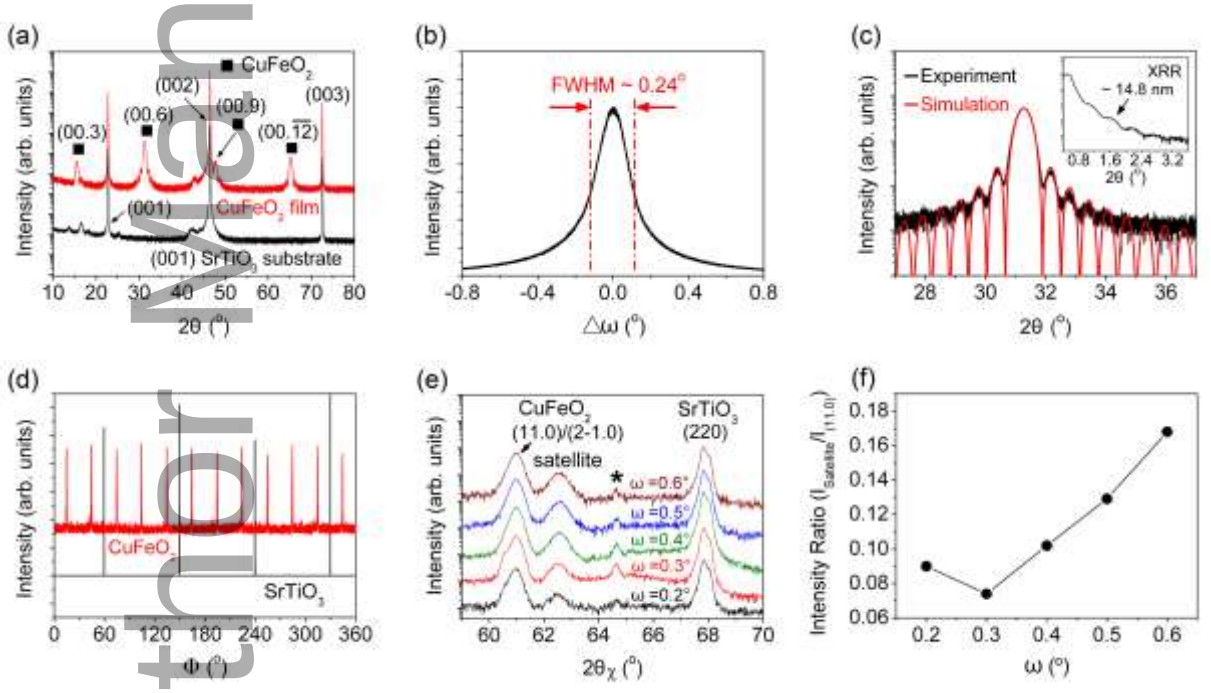

Figure 1. a) XRD pattern of a $CuFeO_2$ thin film deposited on a (001) $SrTiO_3$ substrate, b) rocking curve around the (00.6) peak, c) (00.6) peak and interference fringe simulation with XRR scan in the inset, and d) phi scan of the (01.2) and (013) peaks for the $CuFeO_2$ thin film and the $SrTiO_3$ substrate, respectively. e) In-plane diffraction $2\theta_\chi$-ϕ scans using different incidence angles, ω, from 0.2 to 0.6° (asterisk represents tungsten contamination from X-ray source), f) intensity ratio of the satellite peak versus the (11.0) $CuFeO_2$ Bragg reflection.

Figure 1(a) shows a representative out-of-plane XRD pattern of the $CuFeO_2$ thin films. The 2θ-ω scans were aligned and calibrated using the (002) $SrTiO_3$ reflection at 46.470°

(*a*=3.905 Å). The film exhibits a series of peaks assigned to the (00.3), (00.6), (00.9) and (00.12) planes of the hexagonal delafossite structure of $CuFeO_2$. The rocking curves of the thin film XRD reflexes show a full width at half maximum (FWHM) of about 0.24 degree, as shown in **Figure 1(b)**, suggesting a very good crystalline quality for a heteroepitaxial oxide thin film with a large lattice mismatch of about 10 %. **Figure 1(c)** shows Laue fringes around the (00.6) diffraction peak of a 14.8 nm thick film, with a simulation of fitting the interference fringes.[48] The thickness of film is measured by X-ray reflectivity (XRR), as shown in the insert of **Figure 1(c)**. The evaluated deposition rate of the film is about 0.02 Å per pulse (about 0.37 nm per minute). A (00.1) interplanar distance between two Fe-O layers of one sub-unit cell is evaluated to be 5.714 Å according to the 2θ value of 31.280° for the (00.6) reflections in **Figure 1(a)** and **Figure 1(c)**. The *c*-lattice constant is calculated to be 1.714 nm that is in line with the bulk value range from 1.709 to 1.717 nm,[42,49,50] indicating that there is no significant strain in the films. Considering that the interference fringes are arising from the presence of 26 parallel crystal planes with an interplanar distance of 5.714 Å, the simulation is in a remarkably good agreement with the measurement. The unit cell of layered structure $CuFeO_2$ consists of three sub-unit cells of equal size stacked along the *c*-axis, a total thickness of out-of-plane stacking of 26 sub-unit cells would be about 14.856 nm, which is very close to the evaluated value of 14.8 nm obtained by XRR. These results indicate a very flat surface and interface as well as excellent crystal quality with long range bi-axial order.

The phi scans were performed to determine the in-plane orientation relationship. As shown in **Figure 1(d)**, twelve peaks of $CuFeO_2$ film are separated by 30-degree intervals and are rotated by 15 or 75 degrees with respect to the four peaks from $SrTiO_3$ substrate. This indicates four distinct orientation relationships with the $SrTiO_3$ substrate, which can be denoted as:

$CuFeO_2$ [11.0] // $SrTiO_3$[110] (i)

$CuFeO_2$ [11.0] // $SrTiO_3$[-1-10] (ii)

$CuFeO_2$ [2-1.0] // $SrTiO_3$[-110] (iii)

$CuFeO_2$ [2-1.0] // $SrTiO_3$[1-10] (iv)

The (i) and (ii) relationships as well as the (iii) and (iv) relationships represent mirror inverted variants of each other. The relation between (i) with (iv) and between (ii) with (iii) is a 30° in-plane rotation. This result is similar to the phi scan result of heteroepitaxial ZnO(00.1)/$BaTiO_3$(001) films grown on (001) $SrTiO_3$ substrates,[41] suggesting that a rotational domain heteroepitaxy probably forms between (00.1) $CuFeO_2$ and (001) $SrTiO_3$ crystal planes. From **Figure 1(e)** the in-plane XRD analysis result confirms the presence of the in-plane orientation relationship, and the $CuFeO_2$[11.0]/[2-1.0] directions are parallel to $SrTiO_3$[110] direction. There are completely separate satellite peaks observed near the (11.0) $CuFeO_2$ peaks. **Figure 1(f)** shows the intensity ratios of satellite versus (11.0) $CuFeO_2$ reflection from the data in **Figure 1(e)** as a function of incident angle. As the incident angle, ω increases, the penetration depth of the x-ray also increases, indicating that the satellite peak may originate from deeper in the layer at the interface and may indicate a modulated strain region at the interface.[51] According to the typical interface mode in domain matching epitaxy, the strain is localized in a region at the interface and should relax abruptly within several unit cells (around 1~2 nm) through the formation of a high concentration of interfacial dislocations.

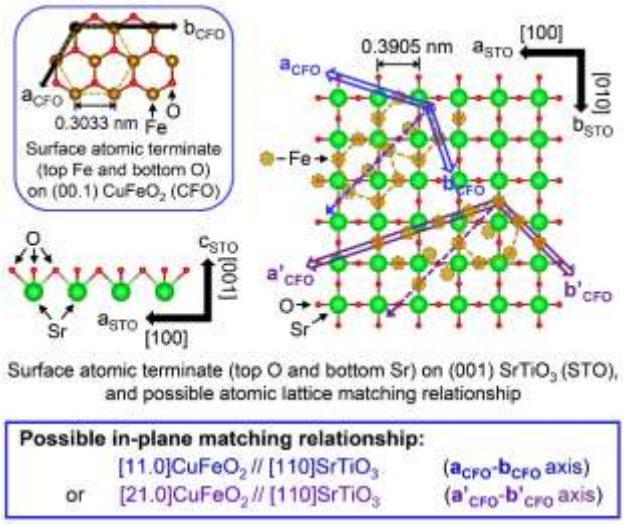

Figure 2. Schematic of atomic scale in-plane lattice matching relationship between (00.1) $CuFeO_2$ and (001) $SrTiO_3$ crystal planes. Crystallographic data of crystal planes and surface

atomic terminations of (00.1) hexagonal delafossite $CuFeO_2$ and (001) cubic perovskite $SrTiO_3$ from Cambridge Structure Database (CSD).[42,43] Atomic-scale structures are visualized using VESTA.[52]

Figure 2 illustrates the atomic-scale schemes of (00.1) $CuFeO_2$ and (001) $SrTiO_3$ crystal planes for revealing in-plane atomic lattice matching. There are two possible in-plane matching relationships: $CuFeO_2$ [11.0] // $SrTiO_3$ [110] and $CuFeO_2$ [21.0] // $SrTiO_3$ [110]. The latter coexists with the orientation relationship of $CuFeO_2$[01.0]//$SrTiO_3$[-110]. The two sets of mirror inverted variants ((i) with (ii) as well as (iii) with (iv)) as discussed above, belonging to the orientation relationships of $CuFeO_2$[11.0]//$SrTiO_3$[110] and $CuFeO_2$[21.0]//$SrTiO_3$[110], present identical Fe terminating planes with the $SrTiO_3$ surface. The in-plane lattice mismatch along $CuFeO_2$[11.0]//$SrTiO_3$[110] direction between (00.1) $CuFeO_2$ (3.033 Å) and (001) $SrTiO_3$ (O-O distance is 2.761 Å) planes is about 10 %. Along the $CuFeO_2$[21.0]//$SrTiO_3$[110] direction, although the lattice misfit is about 90 % with the $SrTiO_3$ lattice, it is about 5 % misfit of one $CuFeO_2$ lattice distance with respect to two $SrTiO_3$ lattice distances for achieving domain matching. While the in-plane lattice mismatch along the $CuFeO_2$[01.0]//$SrTiO_3$[-110] direction is about 10 %. These translational and rotational domain matching relationships are in good agreement with the domain rotation rule in heteroepitaxy.[41] The XPS core-level spectra of Cu2p and Fe2p for the $CuFeO_2$ thin film are shown in **Figure 3**. The film shows a pure Cu^{1+} oxidation state and evidence of Fe^{3+}, suggesting that the film is composed of a pure $CuFeO_2$ phase.[3,4,32,49]

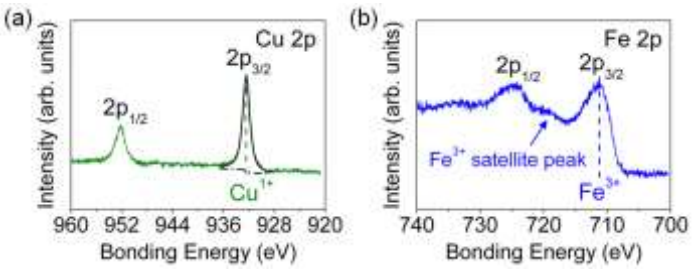

Figure 3. XPS core-level spectra of a) Cu2p and b) Fe2p for the $CuFeO_2$ epitaxial thin film.

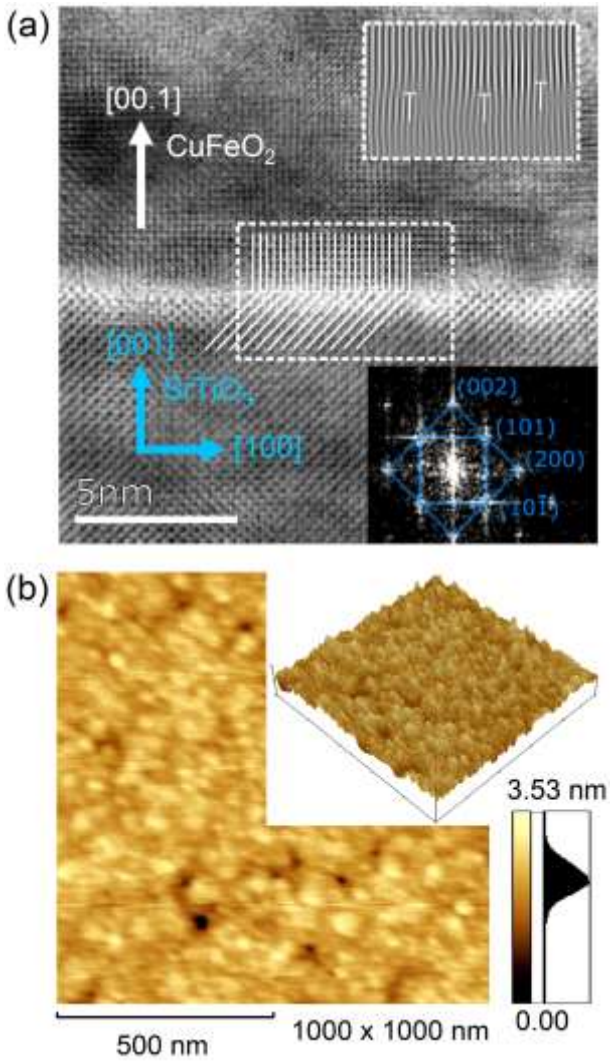

Figure 4. a) Cross-sectional HRTEM image of the 14.8 nm-thick (00.1) $CuFeO_2$ epitaxial thin film grown on a (001) $SrTiO_3$ substrate, the inserted FFT pattern taken from region of substrate with reflections indexed, and the image with annotated lines to help visualize the incoherent interface. b) AFM surface morphology image of the film, with an inserted 3D surface morphology image.

The high-resolution transmission electron microscopy (HR-TEM) was performed to characterize the interface between the $SrTiO_3$ substrate and $CuFeO_2$ thin film. **Figure 4 (a)** shows a HR-TEM interface image with a fast Fourier transform (FFT) of the substrate region. The TEM section was fabricated using a focused ion beam (FIB) using the "lift-out" method. The TEM analysis confirms the thickness of the film and the crystallographic orientation, as measured by XRR and XRD. From the image in **Figure 4 (a)**, the interface appears sharp and incoherent, with no presence of secondary phases observed and significant amounts of strain.

The section marked within the dashed lines has been Fourier filtered and is shown in the inset. An array of edge dislocations is observed along the interface, as expected from the large lattice mismatch between $SrTiO_3$ and $CuFeO_2$. These results are in good agreement with the typical interface characteristic in domain matching epitaxy. **Figure 4 (b)** shows an AFM 2D surface morphology image with an inserted 3D surface morphology image of the epitaxial thin film, which is very similar to the surface morphology of epitaxial (00.1) $CuFeO_2$ thin films with a similar thickness grown on (00.1) sapphire substrates.[32]

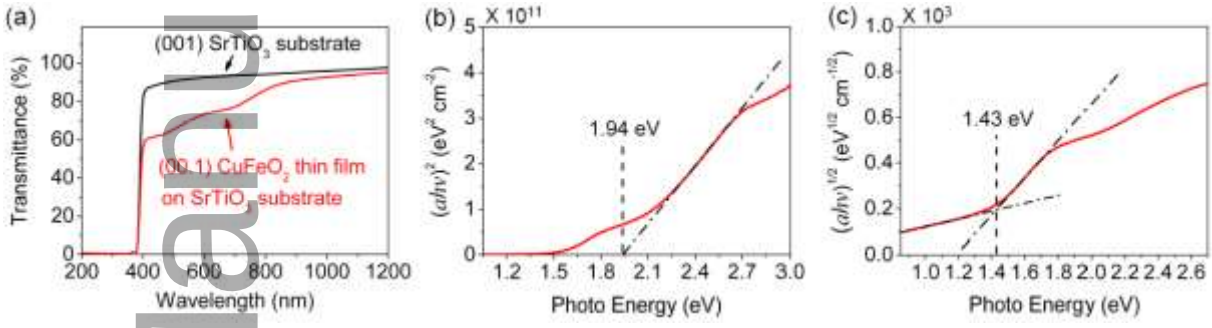

Figure 5. a) UV-Vis-NIR transmission spectrum of the 14.8 nm thick (00.1) $CuFeO_2$ thin film, and b-c) Tauc plots from the transmission spectrum.

Figure 5 shows the UV-Vis-NIR transmission spectrum and the resulting Tauc plots of the 14.8 nm thick (00.1) $CuFeO_2$ epitaxial thin film grown on (001) $SrTiO_3$ substrate. The results are close to the experimental results of the epitaxial (00.1) $CuFeO_2$ thin films grown on sapphire substrates,[32] indicating the high quality, single phase and low defect density of the heteroepitaxial $CuFeO_2$ thin film. The data analysis indicates a possible indirect optical bandgap of 1.43 eV or a possible direct optical bandgap of 1.94 eV, which are consistent with the reports for films prepared by magnetron sputtering showing a 1.43 eV indirect optical bandgap,[12] and the polycrystalline bulk samples exhibiting a direct optical bandgap of 2.03 eV.[1]

In summary, this study demonstrates heteroepitaxial growth of hexagonal (00.1) $CuFeO_2$ thin film on a cubic (001) $SrTiO_3$ substrate through translational and rotational domain matching. The FWHM value of rocking curve of the thin film is about 0.24 degree, and four

distinct in-plane orientation relationships are identified. A 14.8 nm thick film shows a possible indirect optical bandgap of 1.43 eV or direct optical bandgap of 1.94 eV. This work provides new insights into the heteroepitaxial oxide systems with crystallographic symmetry dissimilarity and large lattice mismatch.

Acknowledgements

The authors gratefully acknowledge the support of the International Institute for Carbon Neutral Energy Research (WPI-I^2CNER), sponsored by the World Premier International Research Center Initiative (WPI), MEXT, Japan. G.F.H. gratefully acknowledges financial support from a Kakenhi Grant-in-Aid for Young Scientists (B) Award (no. JP18K13992) and the Platform of Inter/ Transdisciplinary Energy Research Support Program (Q-pit) at Kyushu University. The authors acknowledge the Paul Scherrer Institute (PSI) in Switzerland for support to this work.

Received: ((will be filled in by the editorial staff))
Revised: ((will be filled in by the editorial staff))
Published online: ((will be filled in by the editorial staff))

References

[1] F. A. Benko, F. P. Koffyberg, *J. Phys. Chem. Solids* **1987**, *48*, 431.

[2] R. K. Gupta, M. Cavas, A. A. Al-Ghamdi, Z. H. Gafer, F. El-Tantawy, F. Yakuphanoglu, *Sol. Energy* **2013**, *92*, 1.

[3] A. Bera, K. Deb, T. Bera, S. Sinthika, R. Thapa, B. Saha, *Thin Solid Films* **2017**, *642*, 316.

[4] A. Bera, K. Deb, S. Sinthika, R. Thapa, B. Saha, *Mater. Res. Express* **2018**, *5*, 015909.

[5] C. G. Read, Y. Park, K-S. Choi, *J. Phys. Chem. Lett.* **2012**, *3*, 1872.

[6] J. Gu, A. Wuttig, J. W. Krizan, Y. Hu, Z. M. Detweiler, R. J. Cava, A. B. Bocarsly, *J. Phys. Chem. C* **2013**, *117*, 12415.

[7] M. S. Prevot, N. Guijarro, K. Sivula, *ChemSusChem* **2015**, *8*, 1359.

[8] M. S. Prevot, X. A. Jeanbourquin, W. S. Bouree, F. Abdi, D. Friedrich, R. van de Krol, N. Guijarro, F. L. Formal, K. Sivula, *Chem. Mater.* **2017**, *29*, 4952.

[9] J. Husek, A. Cirri, S. Biswas, A. Asthagiri, L. R. Baker, *J. Phys. Chem. C* **2018**, *122*, 11300.

[10] M. Ferri, J. Elliott, M. F. Camellone, S. Fabris, S. Piccinin, *J. Phys. Chem. C* **2019**, *123*, 29589.

[11] Y. Oh, W. Yang, J. Tan, H. Lee, J. Park, J. Moon, *Adv. Funct. Mater.* **2019**, *29*, 1900194.

[12] C-M. Jiang, S. E. Reyes-Lillo, Y. Liang, Y-S. Liu, G. Liu, F. M. Toma, D. Prendergast, I. D. Sharp, J. K. Cooper, *Chem. Mater.* **2019**, *31*, 2524.

[13] Y. Hermans, A. Klein, H. P. Sarker, M. N. Huda, H. Junge, T. Toupance, W. Jaegermann, *Adv. Funct. Mater.* **2020**, *30*, 1910432.

[14] M. Ferri, J. Elliott, S. Fabris, S. Piccinin, *Phys. Rev. B* **2020**, *101*, 155201.

[15] F. Haydous, M. Döbeli, W. Si, F. Waag, F. Li, E. Pomjakushina, A. Wokaun, B. Gokce, D. Pergolesi, T. Lippert, *ACS Appl. Energy Mater.* **2019**, *2*, 754.

[16] C. Lawley, M. Nachtegaal, J. Stahn, V. Roddatis, M. Döbeli, T. J. Schmidt, D. Pergolesi, T. Lippert, *Nat. Commun.* **2020**, *11*, 1728.

[17] M. Pichler, W. Si, F. Haydous, H. Tellez, J. Druce, E. Fabbri, M. E. Kazzi, M. Döbeli, S. Ninova, U. Aschauer, A. Wokaun, D. Pergolesi, T. Lippert, *Adv. Funct. Mater.* **2017**, *27*, 1605690.

[18] E. W. Burns, D. Pergolesi, T. J. Schmidt, T. Lippert, W. Daramalla, *Chem. Eur. J.* **2020**, *26*, 7065.

[19] E. Burns, U. Aschauer, M. Döbeli, C. W. Schneider, D. Pergolesi, T. Lippert, *J. Mater. Chem. A* **2020**, *8*, 22867.

[20] Q. X. Jia, X. D. Wu, S. R. Foltyn, P. Tiwari, *Appl. Phys. Lett.* **1995**, *66*, 2197.

[21] M. Izuha, K. Abe, M. Koike, N. Fukushima, *Solid State Ionics* **1998**, *108*, 99.

[22] L. J. Sinnamon, R. M. Bowman, J. M. Gregg, *Appl. Phys. Lett.* **2002**, *81*, 889.

[23] K. Khamchane, Y. A. Boikov, Z. G. Ivanov, *Ann. Phys.* **2004**, *13*, 103.

[24] J. Miao, W. R. Chen, L. Zhao, B. Chen, H. Yang, W. Peng, X. H. Zhu, B. Xu, L. X. Cao, X. G. Qiu, B. R. Zhao, *J. Appl. Phys.* **2004**, *96*, 6578.

[25] Y. C. Liang, H. Y. Lee, H. J. Liu, K. F. Wu, T. B. Wu, C. H. Lee, *J. Electrochem. Soc.* **2005**, *152*, F129.

[26] C. S. Liang, H. Y. Chen, J. M. Wu, *Integr. Ferroelectr.* **2006**, *80*, 429.

[27] M. W. Zhu, P. Komissinskiy, A. Radetinac, M. Vafaee, Z. J. Wang, L. Alff, *Appl. Phys. Lett.* **2013**, *103*, 141902.

[28] A. Radetinac, A. Mani, S. Melnyk, M. Nikfalazar, J. Ziegler, Y. Zheng, R. Jakoby, L. Alff, P. Komissinskiy, *Appl. Phys. Lett.* **2014**, *105*, 114108.

[29] P. Salg, D. Walk, L. Zeinar, A. Radetinac, L. Molina-Luna, A. Zintler, R. Jakoby, H. Maune, P. Komissinskiy, L. Alff, *APL Mater.* **2019**, *7*, 051107.

[30] P. Salg, L. Zeinar, A. Radetinac, D. Walk, H. Maune, R. Jakoby, L. Alff, P. Komissinskiy, *J. Appl. Phys.* **2020**, *127*, 065302.

[31] T. Joshi, T. R. Senty, R. Trappen, J. Zhou, S. Chen, P. Ferrari, P. Borisov, X. Song, M. B. Holcomb, A. D. Bristow, A. L. Cabrera, D. Lederman, *J. Appl. Phys.* **2015**, *117*, 013908.

[32] S. Luo, A. Fluri, S. Zhang, X. Liu, M. Döbeli, G. F. Harrington, R. Tu, D. Pergolesi, T. Ishihara, T. Lippert, *J. Appl. Phys.* **2020**, *127*, 065301.

[33] T. Fujii, M. Takano, R. Katano, Y. Bando, Y. Isozumi, *J. Appl. Phys.* **1989**, *66*, 3168.

[34] J. F. Ihlefeld, A. Kumar, V. Gopalan, D. G. Schlom, Y. B. Chen, X. Q. Pan, T. Heeg, J. Schubert, X. Ke, P. Schiffer, J. Orenstein, L. W. Martin, Y. H. Chu, R. Ramesh, *Appl. Phys. Lett.* **2007**, *91*, 071922.

[35] X. H. Wei, Y. R. Li, J. Zhu, W. Huang, Y. Zhang, W. B. Luo, H. Ji, *Appl. Phys. Lett.* **2007**, *90*, 151918.

[36] K. Uehara, A. Okada, A. Okamoto, M. Yokura, S. L. Reddy, S. Kobayashi, K. Inaba, N. Iwata, R. Philip, H. Kezuka, M. Matsui, T. Endo, *Jpn. J. Appl. Phys.* **2012**, *51*, 11PG07.

[37] A. G. Norman, P. C. Dippo, H. R. Moutinho, J. Simon, A. J. Ptak, *Appl. Phys. Lett.* **2012**, *100*, 152106.

[38] S. Luo, G. F. Harrington, K.-T. Wu, T. Lippert, *Phys. Status Solidi RRL* **2020**, *14*, 2000270.

[39] X. H. Wei, Y. R. Li, W. J. Jie, J. L. Tang, H. Z. Zeng, W. Huang, Y. Zhang, J. Zhu, *J. Phys. D: Appl. Phys.* **2007**, *40*, 7502.

[40] M. Brandt, H. Frenzel, H. Hochmuth, M. Lorenz, M. Grundmann, J. Schubert, *J. Vac. Sci. Technol. B* **2009**, *27*, 1789.

[41] M. Grundmann, T. Bontgen, M. Lorenz, *Phys. Rev. Lett.* **2010**, *105*, 146102.

[42] A. M. Sukeshini, H. Kobayashi, M. Tabuchi, H. Kageyama, *Solid State Ionics* **2000**, *128*, 33.

[43] R. J. Nelmes, G. M. Meyer, J. Hutton, *Ferroelectrics* **1978**, *21*, 461.

[44] J. Narayan, B. C. Larson, *J. Appl. Phys.* **2003**, *93*, 278.

[45] M. Zapf, M. Stubinger, L. Jin, M. Kamp, F. Pfaff, A. Lubk, B. Buchner, M. Sing, R. Claessen, *Appl. Phys. Lett.* **2018**, *112*, 141601.

[46] L. Jin, M. Zapf, M. Stubinger, M. Kamp, M. Sing, R. Claessen, C-L. Jia, *Phys. Status Solidi RRL* **2020**, *14*, 2000054.

[47] S. Estandía, N. Dix, M. F. Chisholm, I. Fina, F. Sánchez, *Cryst. Growth Des.* **2020**, *20*, 3801.

[48] J.-M. Triscone, P. Fivat, M. Andersson, M. Decroux, Ø. Fischer, *Phys. Rev. B* **1994**, *50*, 1229.

[49] V. R. Galakhov, A. I. Poteryaev, E. Z. Kurmaev, V. I. Anisimov, S. Bartkowski, M. Neumann, Z. W. Lu, B. M. Klein, T-R. Zhao, *Phys. Rev. B* **1997**, *56*, 4584.

[50] A. Pabst, *Am. Mineral.* **1946**, *31*, 539.

[51] J. Santiso, J. Roqueta, N. Bagués, C. Frontera, Z. Konstantinovic, Q. Lu, B. Yildiz, B. Martínez, A. Pomar, L. Balcells, F. Sandiumenge. *ACS Appl. Mater. Interfaces* **2016**, *8*, 16823.

[52] K. Momma, F. Izumi, *J. Appl. Cryst.* **2011**, *44*, 1272.

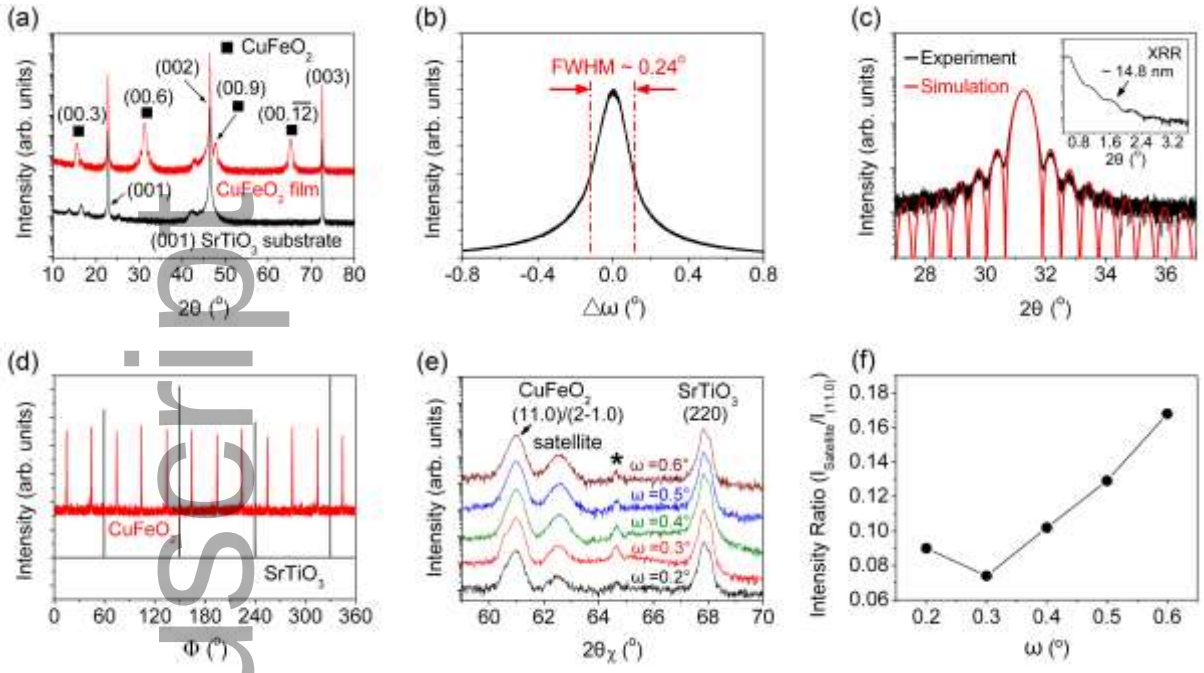

Figure 1. a) XRD pattern of a $CuFeO_2$ thin film deposited on a (001) $SrTiO_3$ substrate, b) rocking curve around the (00.6) peak, c) (00.6) peak and interference fringe simulation with XRR scan in the inset, and d) phi scan of the (01.2) and (013) peaks for the $CuFeO_2$ thin film and the $SrTiO_3$ substrate, respectively. e) In-plane diffraction $2\theta_\chi$-ϕ scans using different incidence angles, ω, from 0.2 to 0.6° (asterisk represents tungsten contamination from X-ray source), f) intensity ratio of the satellite peak versus the (11.0) $CuFeO_2$ Bragg reflection.

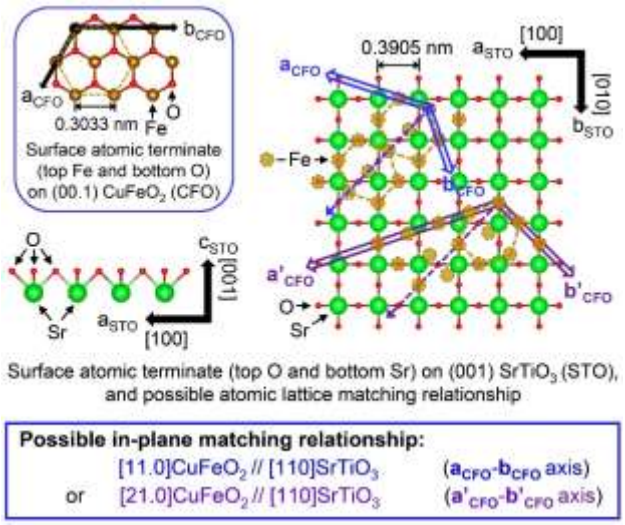

Figure 2. Schematic of atomic scale in-plane lattice matching relationship between (00.1) $CuFeO_2$ and (001) $SrTiO_3$ crystal planes. Crystallographic data of crystal planes and surface atomic terminations of (00.1) hexagonal delafossite $CuFeO_2$ and (001) cubic perovskite $SrTiO_3$ from Cambridge Structure Database (CSD).[38,39] Atomic-scale structures are visualized using VESTA.[48]

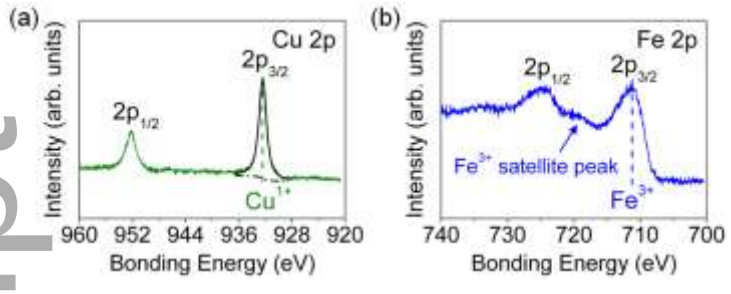

Figure 3. XPS core-level spectra of a) Cu2p and b) Fe2p for the $CuFeO_2$ epitaxial thin film..

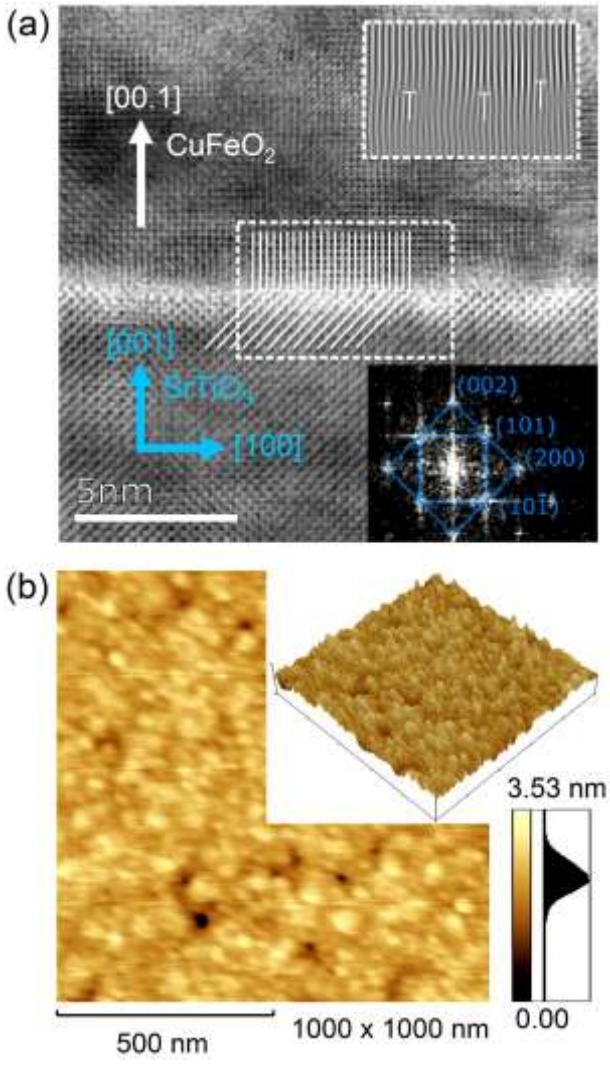

Figure 4. a) Cross-sectional HRTEM image of the 14.8 nm-thick (00.1) $CuFeO_2$ epitaxial thin film grown on a (001) $SrTiO_3$ substrate, the inserted FFT pattern taken from region of substrate with reflections indexed, and the image with annotated lines to help visualize the incoherent interface. b) AFM surface morphology image of the film, with an inserted 3D surface morphology image.

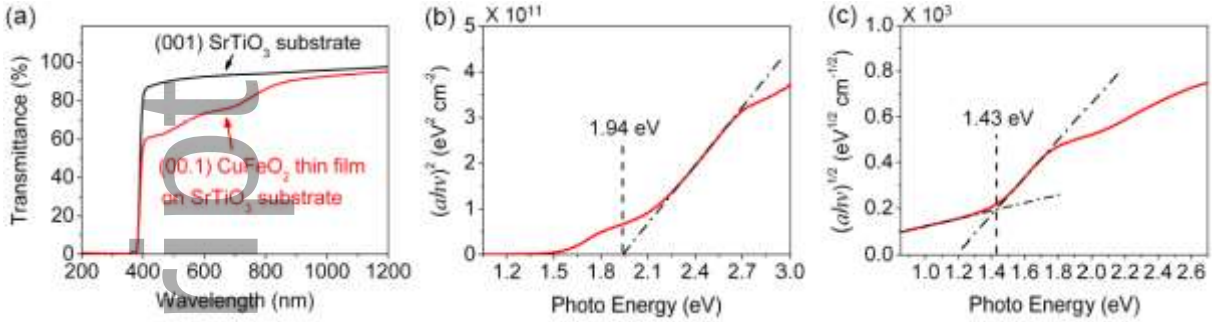

Figure 5. a) UV-Vis-NIR transmission spectrum of the 14.8 nm thick (00.1) $CuFeO_2$ thin film, and b-c) Tauc plots from the transmission spectrum.

The table of contents:

Heteroepitaxial hexagonal (00.1) $CuFeO_2$ thin film grown on a cubic (001) $SrTiO_3$ substrate through translational and rotational domain matching is demonstrated. This study provides new insights into the heteroepitaxial oxide systems with crystallographic symmetry dissimilarity and large lattice mismatch.

Keyword: heteroepitaxial thin films, rotational domain matching, $CuFeO_2$, $SrTiO_3$

S. Luo*, G. F. Harrington*, K.-T. Wu, D. Pergolesi, and T. Lippert*

Title: Heteroepitaxial Hexagonal (00.1) $CuFeO_2$ Thin Film Grown on Cubic (001) $SrTiO_3$ Substrate through Translational and Rotational Domain Matching

ToC figure:

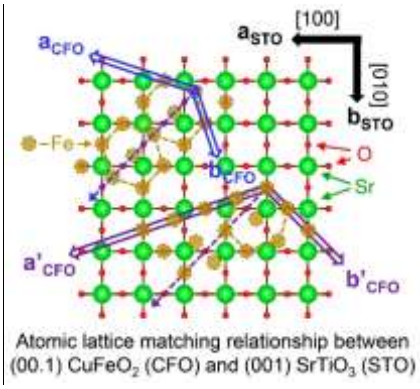

Atomic lattice matching relationship between (00.1) $CuFeO_2$ (CFO) and (001) $SrTiO_3$ (STO)